Earth and Planetary Science Letters 392 (2014) 28–38

Contents lists available at ScienceDirect

Earth and Planetary Science Letters

www.elsevier.com/locate/epsl

Dynamics of the terrestrial planets from a large number of *N*-body simulations

Rebecca A. Fischer *, Fred J. Ciesla

Department of the Geophysical Sciences, University of Chicago, 5734 S Ellis Ave, Chicago, IL 60637, USA

ARTICLE INFO

Article history:
Received 6 September 2013
Received in revised form 26 January 2014
Accepted 3 February 2014
Available online 25 February 2014
Editor: T. Elliott

Keywords:
accretion
N-body simulations
terrestrial planets
Mars
late veneer

ABSTRACT

The agglomeration of planetary embryos and planetesimals was the final stage of terrestrial planet formation. This process is modeled using *N*-body accretion simulations, whose outcomes are tested by comparing to observed physical and chemical Solar System properties. The outcomes of these simulations are stochastic, leading to a wide range of results, which makes it difficult at times to identify the full range of possible outcomes for a given dynamic environment. We ran fifty high-resolution simulations each with Jupiter and Saturn on circular or eccentric orbits, whereas most previous studies ran an order of magnitude fewer. This allows us to better quantify the probabilities of matching various observables, including low probability events such as Mars formation, and to search for correlations between properties. We produce many good Earth analogues, which provide information about the mass evolution and provenance of the building blocks of the Earth. Most observables are weakly correlated or uncorrelated, implying that individual evolutionary stages may reflect how the system evolved even if models do not reproduce all of the Solar System's properties at the end. Thus individual *N*-body simulations may be used to study the chemistry of planetary accretion as particular accretion pathways may be representative of a given dynamic scenario even if that simulation fails to reproduce many of the other observed traits of the Solar System.

© 2014 Elsevier B.V. All rights reserved.

1. Introduction

The canonical view of terrestrial planet formation in our Solar System consists of accretion of increasingly larger bodies in a series of stages. This process began with the collisional and gravitational accumulation of dust and pebbles into planetesimals, bodies measuring tens to hundreds of kilometers in radius (e.g., Cuzzi et al., 2001; Johansen et al., 2007; Weidenschilling, 2003; Youdin and Shu, 2002). Gravitational forces and collisions between these bodies led to the formation of approximately lunar to Mars-mass planetary embryos by runaway accretion (e.g., Wetherill, 1980). The resulting embryos and remaining planetesimals continued to accrete stochastically in a series of large and violent collisions to form the terrestrial planets (e.g., Chambers, 2004; Morbidelli et al., 2012).

The final properties of the planets that form are determined by the ensemble of these various stages of growth. The last stage of planet formation is typically modeled using *N*-body accretion simulations, which begin with a swarm of embryos and planetesimals in orbit around a star, then calculate how their gravitational interactions and collisions lead to the formation of larger planets. This allows us to determine the provenance and timing of accretion of the planetary building blocks, as well as the physical and orbital properties of the resulting planets and how these are set by the dynamic properties of the early Solar System. These results can then be compared to the properties of our terrestrial planets to better understand this process.

Ideally, we could constrain the early dynamical history of the Solar System (e.g., orbital properties of the giant planets) by determining which initial configuration is best able to reproduce all of the properties of the planets. The key properties that were targeted to be reproduced in previous studies included the number, masses, semimajor axes, eccentricities, inclinations, formation timescales, and water contents of the terrestrial planets, as well as the angular momentum deficit (AMD) and radial mass concentration (RMC) of the bulk planetary system, and the mass stranded in the asteroid belt (Raymond et al., 2009). Early low-resolution simulations (e.g., Agnor et al., 1999; Chambers, 2001) with relatively few initial embryos and planetesimals (<160 bodies) were able to approximately reproduce the number, masses, and semimajor axes of the terrestrial planets, despite different initial configurations of the planetary building blocks and the giant planets, suggesting that such outcomes did not depend sensitively on the early dynamics of

* Corresponding author. Tel.: +1 301 512 8871.
E-mail address: rfischer@uchicago.edu (R.A. Fischer).

http://dx.doi.org/10.1016/j.epsl.2014.02.011
0012-821X/© 2014 Elsevier B.V. All rights reserved.

the Solar System. However, these systems tended to produce planets with larger eccentricities and inclinations than the terrestrial planets in our Solar System. O'Brien et al. (2006) and Raymond et al. (2006) demonstrated that similar configurations run at higher resolution (∼50–100 embryos along with >1000 planetesimals) exhibit greater dynamical friction, which damps the eccentricities and inclinations of the embryos and planets, leading to formation timescales and orbital parameters that are more in line with those of the Solar System. Thus it appears that a mix of massive embryos and low mass planetesimals were responsible for producing the planets we see today.

Each of these early studies was able to produce planets that were 'Earth-like' to some extent, in that most simulations produced one planet with nearly the same mass and semimajor axis as that of the Earth. However, it was found that the initial orbital architecture for the planetary building blocks and giant planets used in the simulations had a dramatic effect on other key properties of the planetary system (O'Brien et al., 2006; Raymond et al., 2009). In the cases where Jupiter and Saturn were assumed to exist on their current orbits, the numbers and masses of the terrestrial planets were more easily reproduced, though the planets tended to accrete very little water-bearing materials from the outer edge of the asteroid belt. In those cases where more circular orbits of the giant planets were assumed, consistent with the Nice model (Gomes et al., 2005; Morbidelli et al., 2005; Tsiganis et al., 2005), more water-bearing materials were accreted by the planets, though the masses and numbers did not match the current Solar System. Thus the configuration of the giant planets at the time of terrestrial planet accretion remains uncertain.

While early studies of planet formation largely focused on matching the physical and orbital properties of the planets in our Solar System, the chemical consequences of planetary accretion have also been studied with these same N-body simulations. Two recent studies (Bond et al., 2010; Elser et al., 2012) calculated the compositions of simulated planets to further explore the chemical consequences of planetary accretion, focusing on properties such as their bulk elemental compositions and oxidation states, volatile loss, water delivery, and geochemical ratios. These studies found that the bulk elemental abundances and water contents of the terrestrial planets could be broadly matched in their dynamical studies, though they used only two simulations each, leaving it unclear whether such properties would always be reproduced. When comparing a larger number of simulations or comparing the detailed compositions of the cores and mantles of the simulated planets, even greater variation is expected from simulation to simulation, as a result of the timing of when materials with different compositions were accreted (Rubie et al., 2011). The scatter in accretion histories is thus important to understand in detail as the results of planetary accretion models are highly stochastic, with the final outcomes being strongly dependent on the initial locations of the planetary embryos and planetesimals even in cases where the same general dynamical setting is assumed (e.g., Lissauer, 2007).

Because of the stochastic nature of accretion, it is difficult to evaluate how representative any single run is of the possible accretion histories, and thus final chemical properties, for a resulting planet in a given dynamic scenario. Previous studies performed a small number of N-body simulations, typically four or fewer for each set of initial conditions (Chambers, 2001; Chambers and Wetherill, 1998; Morishima et al., 2010; O'Brien et al., 2006; Raymond et al., 2004, 2006, 2009) and no more than twelve (Raymond et al., 2009). Such a small number of runs is understandable as much earlier studies were limited by computational power, while more recent studies concentrated on exploring parameter space instead of running a large number of simulations per set of conditions (Morishima et al., 2010). Given the range of outcomes that are seen in such simulations, it is not always clear from a limited sample whether a particular constraint is consistently reproduced within a given dynamical environment or if it was a low probability event.

Fully understanding how the early dynamic environment of the Solar System controls the properties of a planetary system or the chemical evolution of a single planet requires that we quantitatively evaluate the range of accretional outcomes and most likely results expected for a particular orbital architecture. This can only be done by performing a statistical analysis of these various starting conditions: rather than focusing on reproducing all observables simultaneously, it is important to know which of the constraints are easily reproduced as well as which constraints are correlated with others for a given dynamical environment. This necessitates performing a large number of simulations in order to determine the probability distribution functions (PDFs) of any given outcome for a given dynamic environment. Only then can we begin to understand the initial configuration of the planetary building blocks in our Solar System.

As our goal is ultimately to utilize N-body simulations to investigate the physical and chemical evolution of the Earth during its formation and early evolution, we want to understand the plausible range of accretion histories of the terrestrial planets in different dynamic settings. Here we carry out a large number of simulations (fifty) for a given set of initial conditions, to quantify the probabilities of reproducing various aspects of the early evolution of the Solar System and especially of the Earth. These simulations provide greater robustness in our evaluation of terrestrial planet accretion models, allowing us to develop a more statistically significant database for analyzing the dynamical outcomes; in particular, it increases our chances for observing low-probability events. Further, our goal is not to reproduce all attributes of the Solar System with these simulations, but instead to determine the correlative relationships between various Solar System properties for different dynamic environments. This allows us to evaluate in detail what this means in terms of using N-body simulations as tools for examining the chemical evolution of the planets in the Solar System. While we focus on just a subset of plausible dynamic environments in the early Solar System, the methodology used here is readily adopted in any other study of planetary accretion.

2. Methods

We performed 100 N-body simulations using the MERCURY code (Chambers, 1999) for two different dynamical environments for the early Solar System (fifty simulations each). The two most commonly tested orbital configurations for the gas giant planets in previous studies are the Eccentric Jupiter and Saturn (EJS) case, where the giant planets are given the orbits that they have today, and the Circular Jupiter and Saturn (CJS) case, where the giant planets are put on non-eccentric orbits as is expected as the starting point in the Nice Model (Gomes et al., 2005; Morbidelli et al., 2005; Tsiganis et al., 2005). These two situations were previously studied by O'Brien et al. (2006) and Raymond et al. (2009), and we follow their approach in setting up the initial conditions for each model, though we increase the resolution slightly by assuming a lower mass for, and thus greater number of, planetesimals. More recent studies have suggested different initial orbital configurations for reproducing the properties of the Solar System (Hansen, 2009; Walsh et al., 2011), which can be explored in future studies. We focus on the EJS and CJS cases to compare and contrast our results with previous studies, which mostly use these configurations. The methodology used here can readily be applied to any other dynamical environment of interest.

Each simulation began with ∼80 embryos, following a solid disk surface density profile of $\Sigma(r) = \Sigma_0(r/1\ \mathrm{AU})^{-3/2}$ (Weidenschilling, 1977), with $\Sigma_0 = 10\ \mathrm{g/cm^2}$. There were also ∼2000 plan-

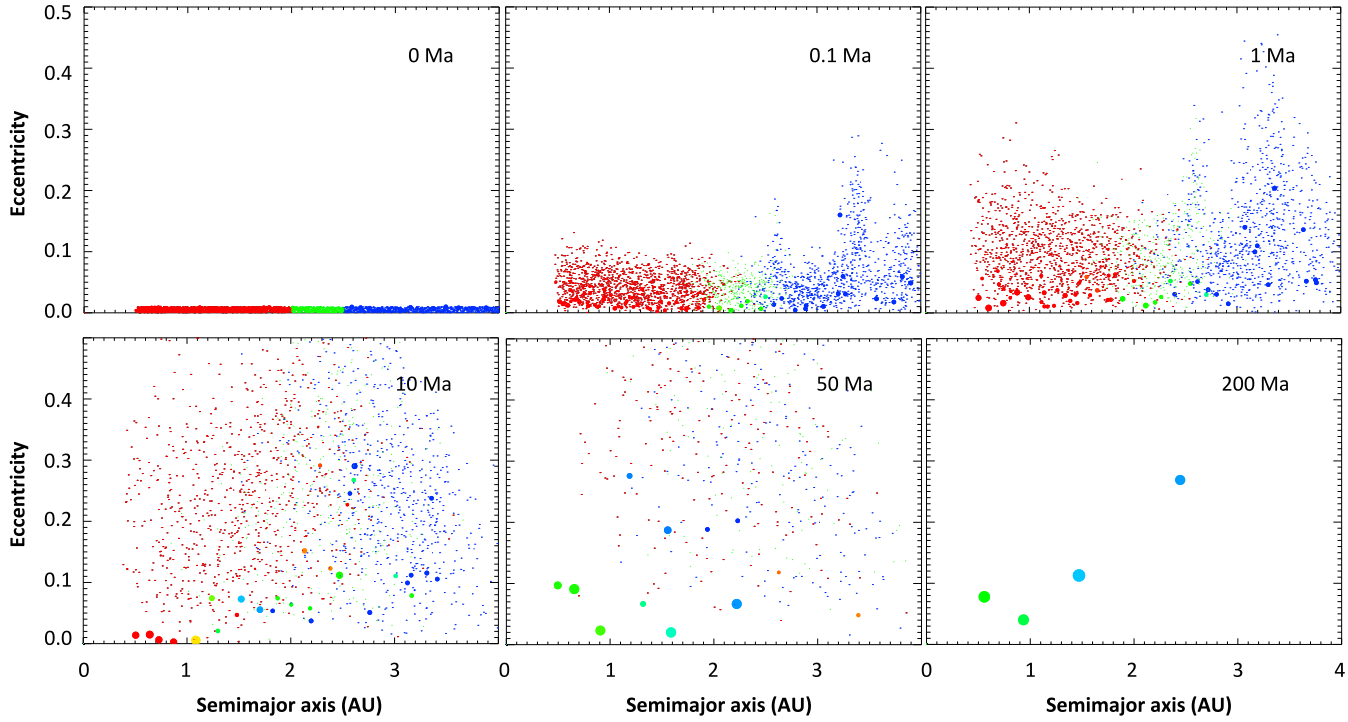

Fig. 1. Orbital evolution of simulated bodies in simulation CJS33. Time series are shown at 0, 0.1, 1, 10, 50, and 200 Ma after the start of the simulation. Red bodies originated inside of 2 AU, green bodies between 2 and 2.5 AU, and blue bodies outside of 2.5 AU, illustrating the initial water distribution in our model. Intermediate colors at later times indicate intermediate water contents. Larger circles are planetary embryos, while smaller circles are planetesimals. (For interpretation of the references to color in this figure legend, the reader is referred to the web version of this article.)

etesimals, with the total mass of the system divided equally between the two populations. Planetesimals had masses of ∼0.001 $M_\oplus$, while the masses of planetary embryos were determined by Σ_0 and their spacing, with masses increasing with increasing distance from the Sun (e.g., Chambers and Wetherill, 1998; Raymond et al., 2009). In our simulations, we initially distributed planetary embryos with a spacing of seven mutual Hill radii, leading to masses in the range 0.01–0.06 $M_\oplus$. All embryos and planetesimals were given densities of 3 g/cm^3. These initial conditions are similar to those used in other recent studies (e.g., Morishima et al., 2010; Raymond et al., 2009).

Planetary embryos interacted with each other and with planetesimals, but planetesimal–planetesimal interactions were not included. All bodies were initially located between 0.5 and 4 AU. Initial eccentricities were chosen randomly between values of zero and 0.01, and inclinations were set to different random values between zero and 0.01 degrees. Other orbital parameters (argument of pericenter, longitude of ascending node, and mean anomaly) were assigned randomly. For each of the fifty cases considered for the EJS and CJS environments, the semimajor axes of the embryos and planetesimals were held constant, while the rest of their orbital arguments varied randomly from case to case. The initial distribution of embryos and planetesimals from one of our simulations is shown in the first panel of Fig. 1.

Each simulation is integrated for 200 Ma with a timestep of six days. Collisions are treated as inelastic mergers, occurring when two bodies pass within a distance that is less than the sum of their radii. Collisions are assumed to result in perfect merger, with the resulting body's mass and momentum taken to be the sum of those of the two bodies at the time of impact. This is an approximation, since many collisions were likely hit-and-run or erosive impacts instead of perfect accretion events (e.g., Asphaug, 2010). Nonetheless, recent studies (Chambers, 2013; Leinhardt et al., 2009) demonstrated that fragmentation does not have a large effect on the final physical properties of the planetary system, with the most important difference being a slight increase in the duration of accretion. The chemical consequences of fragmentation, however, will be investigated in future studies.

3. Results and discussion

Fig. 1 shows a time series of the orbital evolution of the bodies formed in one of our CJS simulations. Bodies are color-coded according to their initial locations (red inside 2 AU, green between 2 and 2.5 AU, and blue outside 2.5 AU). Such differences in starting location could represent differences in composition, though details of spatial gradients in the composition of planetary building blocks are very uncertain. For example, this could correspond to a change in water content, as has been used in previous studies of water delivery to terrestrial planets (e.g., Morbidelli et al., 2000; O'Brien et al., 2006; Raymond et al., 2004, 2006, 2009). As early as 0.1 Ma into the simulation, resonances from Jupiter and Saturn are visible in the form of spikes in eccentricity at ∼2.6 AU and ∼3.3 AU. Eccentricities further increase at later times, with planetesimals having larger eccentricities than planetary embryos due to dynamical friction (O'Brien et al., 2006). By 10 Ma, there are fewer bodies and they continue to grow, exhibiting variations in size and composition. Some features of this simulation are nearly universal across all of our runs, such as the increased eccentricities at certain resonance locations and lower eccentricities for larger bodies, though the final outcomes of the simulations (such as the number of bodies produced and their masses) vary (Supplemental Fig. 1).

Our ultimate goal is to understand the physical and chemical evolution of the simulated planets. Here we investigate the distributions of accretion histories and outcomes in our dynamical simulations, with a particular focus on quantitatively exploring the details of the Earth's accretion and correlations between observables in these environments.

3.1. Comparisons to the Solar System

To begin, we focus on the properties of the final planetary system, following Raymond et al. (2009) in quantifying a set of parameters that are typically used to compare N-body simulations and evaluate their ability to reproduce the Solar System. We use definitions of Solar System planetary analogues from Raymond et al. (2009), for the purpose of evaluating the success of our simulations at reproducing the terrestrial planets. The Earth analogue is taken to be the largest planet between 0.75 and 1.25 AU. If there is no planet within this range, the Earth analogue is the closest planet to 1 AU. The Mars analogue is the smallest planet in the range 1.25–2 AU outside of the Earth analogue's orbit. We define a planet as a body containing at least one embryo after 200 Ma of evolution.

Supplemental Tables S1 and S2 display the results of each of our EJS and CJS simulations, respectively, and compare key quantities in these simulations to Solar System values. In addition to outcomes for each simulation, these tables include statistical data (average value, standard deviation, and range) for each property, the Solar System value, the definition we use for a match to the Solar System value, and the percentage of simulations that meet that definition. Table 1 summarizes these results.

3.1.1. Orbital architecture of the final planetary system

The properties of the final planetary systems that we quantify include the angular momentum deficit (AMD), or the portion of the Solar System's angular momentum resulting from non-circular and non-planar orbits (Laskar, 1997); the radial mass concentration (RMC), which measures the extent to which mass is concentrated in one region of the Solar System, such as in the range of semi-major axes near Earth and Venus (Chambers, 2001); and the mass of bodies remaining in the asteroid belt. The angular momentum deficit is defined as:

$$AMD = \frac{\sum_j m_j \sqrt{a_j}(1-\cos(i_j)\sqrt{1-e_j^2})}{\sum_j m_j \sqrt{a_j}} \quad (1)$$

where m_j, a_j, i_j, and e_j are the mass, semimajor axis, inclination, and eccentricity, respectively, of planet j (Laskar, 1997). The radial mass concentration (RMC, Raymond et al., 2009, sometimes referred to as S_C) is defined as:

$$RMC = \max\left(\frac{\sum_j m_j}{\sum_j m_j[\log_{10}(a/a_j)]^2}\right) \quad (2)$$

AMD and RMC values for our simulations are summarized in Table 1. The average value we find for AMD is closer to that of the Solar System than was found by Raymond et al. (2009) and Morishima et al. (2010), though still high and with a similarly large standard deviation, and farther from the Solar System value than that reported by O'Brien et al. (2006). RMC values of the EJS simulations provide a better match to the Solar System value, consistent with the results of Raymond et al. (2009). The Solar System RMC value lies ~3 standard deviations from the mean in our EJS simulations, whereas it is ~5 standard deviations from the mean in the CJS simulations. Thus, this particular outcome is difficult to reconcile in models with giant planets on circular orbits and is more easily produced with those planets on eccentric orbits. This finding is also consistent with the results of Morishima et al. (2010).

In addition to the orbits of the planets, the structure of the asteroid belt provides some constraints on the early dynamical evolution of the Solar System. The lack of gaps besides those caused by specific mean motion or secular resonances implies that less than a few lunar masses of material were stranded in the asteroid belt after planetary formation

Table 1
Summary of results from EJS and CJS simulations. All times are given in Ma and masses in $M_\oplus$. T_F, formation timescale. See text for definitions of the parameters. Solar System values are taken from Dauphas and Marty (2002), Krasinsky et al. (2002), Nimmo and Kleine (2007), Raymond et al. (2009), Schlichting et al. (2012), and Touboul et al. (2007).

	Solar System values	Definition of match	EJS				CJS			
			Mean	Standard deviation	Range	Percent that match	Mean	Standard deviation	Range	Percent that match
AMD	0.0018	0.0009–0.0036	0.0034	0.0039	0.0002–0.0195	50	0.0045	0.0047	0.0004–0.0249	30
RMC	89.9	44.9–179.8	40.9	14.6	18.9–114.0	24	34.6	10.8	22.8–70.6	12
WMF	>0.001?	>0.0003	0.0015	0.0020	0.0001–0.0098	74	0.0052	0.0036	0.0008–0.0135	100
T_F Earth	50–150	50–150	61.5	38.9	10.9–174.8	42	82.6	41.5	5.6–184.9	68
Mass in asteroid belt	0.0006	<0.05	0.13	0.14	0–0.62	26	0.31	0.30	0–1.46	16
Late veneer mass	0.001–0.01	0.0005–0.02	0.038	0.033	0.001–0.140	42	0.032	0.036	0–0.196	40
Mars mass	0.11	<0.22				10				4
T_F Mars	<10	<20				14				8

(Raymond et al., 2009), a criteria that is difficult to meet in many accretion simulations, as most have left greater mass of material than this. Therefore, the mass left in the asteroid belt at the end of a simulation may serve as a test of the simulated planetary system's similarity to the Solar System. The criteria used in this study (<0.05 $M_\oplus$ remaining in the asteroid belt after 200 Ma) is taken from Raymond et al. (2009) and is possibly higher than the actual mass that existed there after terrestrial planet formation, given the magnitudes of the depletions caused by the Late Heavy Bombardment and chaotic diffusion (e.g., Fassett and Minton, 2013; Gomes et al., 2005; Minton and Malhotra, 2009, 2011). More than three-quarters of our simulations ended with too much mass in this region (Table 1). An EJS configuration is slightly more successful than a CJS configuration at clearing the asteroid belt, matching Solar System constraints in 26% of the cases as opposed to 16%. However, the differences in these outcomes in our model are not as strong as the contrast between the EJS and CJS results as reported by Morishima et al. (2010), who found that eccentric giant planets were much more efficient at depleting the mass of the asteroid belt.

3.1.2. Formation of Mars

A long-standing issue in planetary accretion simulations has been the formation of Mars, as most simulations produce planets near Mars's orbit that are much more massive than the actual planet. As a result, efforts have focused on defining dynamical environments that consistently produce a low mass planet around 1.5 AU. Among the ideas now discussed is that the terrestrial planets formed from a narrow annulus of planetesimals which orbited in the range 0.7–1.0 AU, allowing Mars to form from a region which was limited in its available mass of solid bodies (Hansen, 2009). This annulus of planetesimals may have resulted from the inward then outward migration of Jupiter (Walsh et al., 2011).

While our models also typically produce planets at Mars's location that are much larger than the planet, we do find that the probability of producing a small planet in this region is not zero (Table 1). This can be seen in Fig. 2, which shows the relationship between mass and semimajor axis of all planets produced in all of our simulations. Here, 14% of our EJS simulations, and 4% of our CJS simulations, produce a planet that is less than 0.2 $M_\oplus$ in the 1.25–2 AU region, our definition of Mars analogues. If only four simulations were performed, as typically done in previous studies, there would be a 55% and 85% likelihood of not seeing such Mars analogues using EJS and CJS configurations, respectively. These results are in agreement with Raymond et al. (2009), who also found that Mars analogues are more common in EJS runs.

These low mass planets represent embryos that have escaped embryo–embryo accretion events. Constraints on Mars's accretion history have come from analyses of Martian meteorites, where it has been inferred that Mars accreted to 80% of its final mass in the first 2 Ma of Solar System history, assuming that any iron added to the planet fully equilibrated with the mantle before being incorporated into the embryo's core (Dauphas and Pourmand, 2011). Incomplete equilibration would allow longer accretion timescales, though it is unlikely Mars formed after 10 Ma (Nimmo and Kleine, 2007).

Adopting these constraints and defining a planet's formation timescale to be the time of the last planetary embryo accretion, we find that 10% of our EJS simulations and 2% of our CJS simulations (only one simulation) form a planet that approximately matches Mars in terms of its mass, formation timescale, and semimajor axis simultaneously (Table 1). Thus the formation of Mars, as we currently understand it, is not excluded in these dynamic scenarios, but it is a very low probability event that would likely not be seen if only 4–5 simulations were performed.

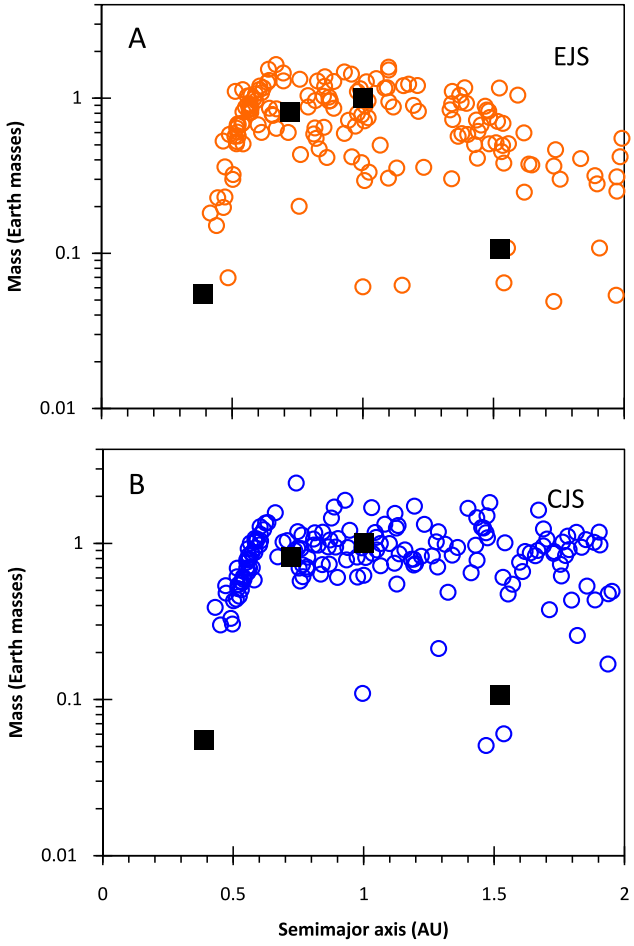

Fig. 2. Mass versus semi-major axis of all planets produced in all fifty A: EJS simulations and B: CJS simulations. Open circles are simulated planets; black filled squares are Solar System terrestrial planets.

3.1.3. Formation of Earth

While the vast majority of our simulations form a planet that meets our criteria of an Earth analogue in terms of its mass and semimajor axis (Section 3.1.1), we can also evaluate the success of our simulations more closely in terms of these parameters, as well as the formation timescale, water content, and late veneer mass of the Earth analogue. We can then use these simulations to explore possible accretional histories of the Earth, the fraction of Earth's mass from embryos versus planetesimals, and the origins of the building blocks of the Earth (Section 3.3).

We find that 84% of EJS simulations and 92% of CJS simulations produce an Earth analogue that simultaneously matches the Earth's mass within a factor of two and semimajor axis within the range 0.75–1.25 AU. The moon-forming impact on the Earth, which is thought to be the last major impact that the Earth experienced, likely occurred 50–150 Ma after Solar System formation (Touboul et al., 2007). In our simulations, the final accretion event involving an embryo striking the Earth analogue ranges from 5.6 to 184.9 Ma. CJS conditions lead to slightly later formation times for Earth on average (Table 1), and meet this constraint in 68% of cases as opposed to 42% for the EJS runs.

Though the water content of the Earth is not precisely known, it is at least as large as the mass of the surface oceans. A variety of mechanisms have been proposed to account for the Earth's water budget, with many studies favoring the delivery of water from asteroidal material (e.g., Albarede et al., 2013; Alexander et al., 2012; Morbidelli et al., 2000; Raymond et al., 2009), which we consider here. We assign the water contents of planetary embryos and

Table 2
Correlation matrix of various Solar System observables from our fifty EJS simulations. Each cell contains the Pearson correlation coefficient r (see text for definition) for the properties defining the row and column that intersect at its location. A value of −1 indicates a perfect negative linear correlation, zero represents no correlation, and +1 is a perfect positive correlation. Formation of Mars in each simulation was assigned a value of 0 or 1, depending on whether or not an analogue formed that matched all required properties (see Table 1).

	AMD	RMC	WMF	T_F Earth	Asteroid belt mass	Late veneer mass	Formation of Mars
AMD	1	0.06	0.56	0.28	0.00	−0.28	0.00
RMC	0.06	1	−0.09	0.03	0.27	−0.28	0.22
WMF	0.56	−0.09	1	0.2	0.15	−0.3	0.00
T_F Earth	0.28	0.03	0.2	1	0.11	−0.74	0.04
Asteroid belt mass	0.00	0.27	0.15	0.11	1	−0.11	−0.04
Late veneer mass	−0.28	−0.28	−0.3	−0.74	−0.11	1	−0.14
Formation of Mars	0.00	0.22	0.00	0.04	−0.04	−0.14	1

Table 3
Correlation matrix for CJS simulations (analogous to Table 2).

	AMD	RMC	WMF	T_F Earth	Asteroid belt mass	Late veneer mass	Formation of Mars
AMD	1	0.05	0.03	0.3	−0.12	−0.16	0.01
RMC	0.05	1	0.23	0.43	0.77	−0.32	0.06
WMF	0.03	0.23	1	0.2	0.13	−0.31	0.33
T_F Earth	0.3	0.43	0.2	1	0.19	−0.73	−0.05
Asteroid belt mass	−0.12	0.77	0.13	0.19	1	−0.19	−0.02
Late veneer mass	−0.16	−0.32	−0.31	−0.73	−0.19	1	−0.02
Formation of Mars	0.01	0.06	0.33	−0.05	−0.02	−0.02	1

planetesimals based on their initial positions following the model of Raymond et al. (2009), with a water mass fraction (WMF) of 10^{-5} inside 2 AU, 10^{-3} between 2 and 2.5 AU, and 5% outside 2.5 AU. The WMF of a growing planet was calculated with each accretion event using a mass balance equation, assuming no water loss during impact. Under these assumptions, many of our planets formed with substantial quantities of water (Table 1). CJS simulations produced significantly more water-rich Earth analogues than EJS runs, containing an average of 0.0052 ± 0.0036 $M_\oplus$ of water versus 0.0015 ± 0.0020 $M_\oplus$. This is likely due to the efficient removal of water-rich bodies by gravitational scattering from Jupiter and Saturn in EJS simulations, consistent with previous studies (O'Brien et al., 2006; Raymond et al., 2004, 2009). However, an important caveat with these simulations is that there are large uncertainties associated with the initial water contents of planetary building blocks, the amount of water loss in collisions, and the water content of the Earth for comparison, as considerable water may be stored in the mantle (e.g., Karato, 2011). Nonetheless, CJS runs appear to deliver larger amounts of mass from the outer regions of the terrestrial planet zone to the Earth analogue than do EJS simulations (Section 3.3).

The late veneer refers to the hypothesized late delivery of material to the Earth, to explain the highly siderophile element abundances, and their chondritic relative abundances, in the Earth's mantle (Morgan, 1986). The late veneer was likely delivered in small bodies to avoid loss of material to the Earth's core. The mass of the late veneer has been estimated to be in the range 0.0009–0.005 $M_\oplus$ (Dauphas and Marty, 2002; Mann et al., 2012; Walker, 2009), or possibly as large as 0.01 $M_\oplus$ (Schlichting et al., 2012). We define the late veneer mass to be the mass of planetesimals accreted by the Earth analogue after the accretion of the last planetary embryo (at times later than the formation timescale). In nearly half of our simulations, Earth accretes a late veneer whose mass is within the range 0.0005–0.02 $M_\oplus$. This finding is broadly consistent with the results of Raymond et al. (2013). The average late veneer masses for EJS and CJS runs are very similar (Table 1). This indicates that the late veneer mass is somewhat independent of the orbits of Jupiter and Saturn, at least when comparing EJS and CJS cases. However, the provenance of the late veneer is sensitive to the giant planet configuration (Section 3.3).

3.2. Correlations between Solar System observables

While we have quantified the fraction of simulations that reproduce particular Solar System constraints on planetary accretion, it is important to consider whether pairs of observations reproduced in simulations are correlated with one another when evaluating a possible dynamic environment and its effects on planetary formation and chemistry. If matching one variable makes it impossible to match another, then the starting conditions may not accurately represent those of the Solar System. If there is no correlation between the accretion outcomes, then one cannot dismiss the evolutionary pathway of the Earth analogue in a given model run simply because another feature of the Solar System (e.g., Mars mass, RMC, asteroid belt mass) was not reproduced.

Tables 2 and 3 show the correlation matrices for our EJS and CJS simulations, respectively. Each entry represents the correlation between the observables corresponding to the row and column that intersect at its location. The matrices contain Pearson correlation coefficients r, which are calculated as:

$$r = \frac{\sum_{i=1}^{50}(X_i - \bar{X})(Y_i - \bar{Y})}{\sqrt{\sum_{i=1}^{50}(X_i - \bar{X})^2}\sqrt{\sum_{i=1}^{50}(Y_i - \bar{Y})^2}} \quad (3)$$

where X and Y represent the two observables being tested, X_i and Y_i are individual data points, $\bar{X}$ and $\bar{Y}$ are the mean values of those observables, and all sums are performed over our fifty simulations for each dynamic environment. Values of r range from −1 (perfect negative correlation) to +1 (perfect positive correlation), with a value of zero representing no correlation. By definition these matrices (Tables 2 and 3) are symmetric with values of 1 on the diagonals. Pearson coefficients test for linear relationships between the two variables; however, inspection of plots of all iterations of variables reveals that there are no additional types of correlations that were undetected by the Pearson coefficients. Definitions of "strong" versus "weak" coefficients vary; in the following discussion, we consider an r value of >0.6 (absolute value) to indicate a strong correlation, 0.35–0.6 a moderate correlation, 0.2–0.35 a weak correlation, and <0.2 no or negligible correlation.

In our EJS simulations (Table 2), the strongest correlation is between the mass of the late veneer and the formation timescale of the Earth (Fig. 3C). This negative correlation ($r = -0.74$) is to be expected: if the final giant impact on the Earth occurs late, there

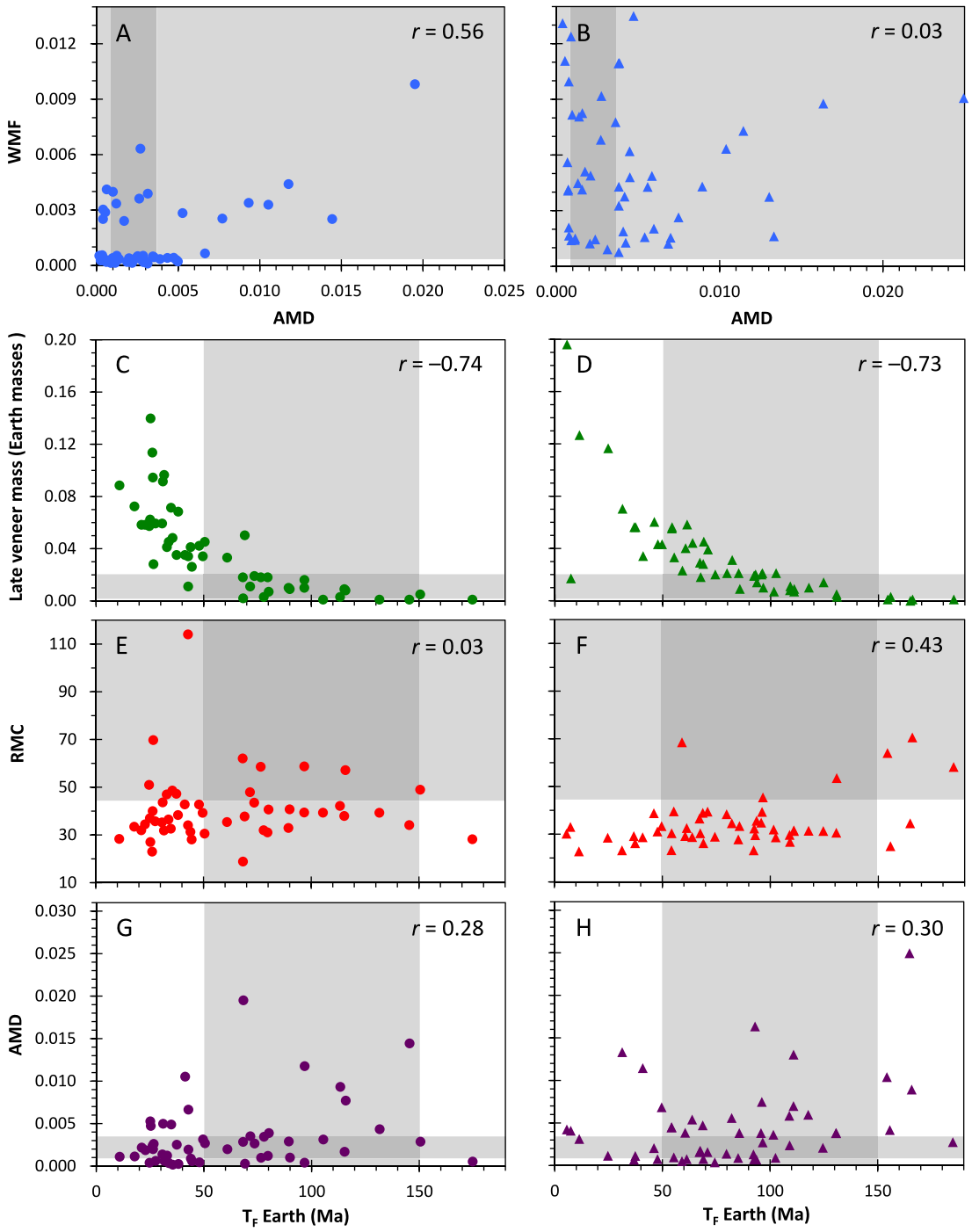

Fig. 3. Correlations between observables from EJS (circular symbols, parts A, C, E, and G) and CJS (triangular symbols, parts B, D, F, and H) simulations. A and B: Angular momentum deficit versus the water mass fraction of the Earth analogue, illustrating a positive correlation that is somewhat skewed by one data point in the EJS simulations and no correlation in the CJS simulations. C and D: Late veneer mass versus formation timescale of Earth, showing a strong negative correlation (see text for discussion). E and F: Radial mass concentration versus Earth formation timescale, which exhibit no correlation (EJS simulations) or a positive correlation (CJS simulations). G and H: Angular momentum deficit versus the formation timescale of the Earth, showing a weak positive correlation. Shaded regions indicate our definition of a match (Table 1).

are fewer planetesimals remaining for the Earth to accrete as part of its late veneer, whereas there are more planetesimals available to be accreted at earlier times. A moderate correlation in our EJS simulations is seen between the angular momentum deficit and the water mass fraction of the Earth, with $r = 0.56$ (Fig. 3A). However, this is somewhat skewed by the presence of one data point at high AMD and high WMF; removing this point lowers r to 0.30. No other combinations of observables produce r values with absolute values greater than 0.3 in our EJS simulations, indicating weak or no correlations between any other properties. For example, the radial mass concentration and the formation timescale of the Earth have an r value of 0.03 (Fig. 3E), indicating that any Earth formation timescale may be allowed for a given radial mass concentration value.

Our CJS simulations (Table 3) similarly show a strong negative correlation between late veneer mass and Earth formation timescale (Fig. 3D), with $r = -0.73$, for the same reasons as in the EJS runs. AMD and WMF show no correlation ($r = 0.03$; Fig. 3B), somewhat consistent with the low correlation of the EJS simulations if the one outlying data point were removed. In contrast to

the results of the EJS runs, the CJS simulations show a moderate correlation ($r = 0.43$) between RMC and the formation timescale of the Earth (Fig. 3F). We also find a correlation between RMC and asteroid belt mass ($r = 0.77$), which are only weakly correlated in our EJS results ($r = 0.27$). No other pairs of observables in CJS runs produce r values greater than ± 0.35, indicating weak or no correlations between any other properties.

Morishima et al. (2010) observed a strong correlation between RMC/$a_{\rm m}^2$ (where $a_{\rm m}$ is the mass-weighted mean semimajor axis) and the formation timescale of Earth, combining simulation results using various initial conditions (different configurations of Jupiter and Saturn and different values of the gas decay rate, surface density of planetesimals, and initial mass of planetesimals). We see no correlation between RMC and Earth formation time in EJS runs, but a moderate correlation in CJS runs that may be the source of the correlation that Morishima et al. (2010) reports (Fig. 3E and F). These observations could be explained by less efficient scattering and removal of bodies in the CJS runs compared to EJS runs. More mass in the outer terrestrial planet region allows for more prolonged accretion timescales and the formation of larger planets far from the Sun in CJS runs. This same effect could explain the stronger correlation between RMC and asteroid belt mass seen in CJS runs as bodies would remain in the outer terrestrial planet region either as members of the asteroid belt or by being accreted into a planet. The more efficient scattering and removal of bodies in the EJS runs would prevent these correlations from developing.

We observe a weak correlation between formation timescale of the Earth and angular momentum deficit: $r = 0.28$ for EJS simulations and 0.30 for CJS simulations (Fig. 3G and H, respectively). Morishima et al. (2010) found a strong trade-off between these parameters, concluding that the final giant impact on Earth needs to occur early to avoid producing a very high angular momentum deficit. Our values for AMD are generally higher than the Solar System value, with mean values in the EJS and CJS cases being 2 and 2.5 times that of the observed value (Table 1), and we do find a positive correlation between AMD and Earth formation timescale. However, the weak correlation found in our statistical analysis reveals that this correlation is not strong enough to deem these simulations to be unfit to represent Solar System formation; that is, a late formation time of the Earth does not preclude a low value of the AMD.

3.3. Applications of N-body simulations

One of our main goals is to evaluate the applicability of these N-body simulations to understanding physical and chemical processes during the early evolution of the Earth. To do this, we need to determine whether our simulations may provide representative descriptions of how the Earth accreted.

Table 1 lists the probabilities of matching various Solar System observables for the EJS and CJS simulations we ran. Given the number of parameters tested and the modest probabilities of a match, a very large number of simulations would need to be run to match every observable simultaneously. For an EJS environment, the probability of matching all observables listed in Table 1 is 5.7×10^{-5}, meaning that an average of nearly 18,000 simulations would need to be run to find one that produces outcomes matching all of the listed constraints from our Solar System. Similarly, for a CJS configuration, the probability of matching all of these properties is 5.0×10^{-6}, corresponding to an average of nearly 200,000 runs needed to produce one that matches the Solar System. Given these extremely low probabilities, and the unrealistically large number of simulations that would need to be run to simultaneously match all Solar System observables that we tested (Table 1), it is not practical to run simulations until all observables are matched to determine how the Earth accreted its mass.

However, the lack of correlations between the various Solar System outcomes considered here (Tables 2 and 3) implies that if we are interested in understanding the distribution of results for one particular observable, we do not have to run simulations until all Solar System properties are reproduced. That is, if a given simulation fails to produce a Mars analogue with sufficiently low mass, it does not preclude the Earth analogue of that simulation from accreting the proper water fraction, because these variables are uncorrelated. Thus, any of the Earth accretion histories produced in these simulations should be considered viable representations of Earth's formation for these particular dynamic environments that can be used to understand the physics and chemistry of its accretion.

Studies are beginning to use N-body simulations as a means of predicting the bulk chemistry of planets (e.g., Bond et al., 2010; Elser et al., 2012). Other studies using more complex chemical models to consider the partitioning of elements between a planet's core and mantle (Rubie et al., 2011) could be made more realistic by coupling their chemical models to N-body accretion simulations. Such simulations offer distinct advantages over the use of an artificial growth scenario because they provide information about realistic mass evolution pathways of planets; whether mass originated as planetesimals or embryos, and thus the degree of reequilibration expected upon impact; and the provenance of the accreted material, which determines its initial chemistry.

By running a large number of simulations, we can better observe the range and distribution of possible mass evolution pathways of the Earth in the dynamic environments considered here. Fig. 4 illustrates the wide range seen in our fifty EJS simulations. Most pathways exhibit periods of very slow growth as the Earth accreted planetesimals, punctuated by large jumps in mass fraction (sometimes exhibiting increases of almost 50% of the final mass) due to the accretion of planetary embryos, many of which have rich accretion histories of their own.

We can also get a statistical sense of the nature and origins of the building blocks of the Earth. For example, 57% $\pm$ 6% (one standard deviation) of the Earth analogue's mass comes from bodies that began as planetary embryos in the EJS simulations, with the remainder from planetesimals. In the CJS runs, 53% $\pm$ 6% of Earth's mass originated in embryos. These values are the same within uncertainty, and these distributions are illustrated in Fig. 5. The total percentage of the Earth analogue that originated as planetary embryos ranges from 41% to 79%.

Fig. 6 shows the mass fraction of the Earth analogue accreted from various initial semimajor axes in our EJS and CJS simulations. The average distribution shows a nearly monotonic decrease in mass fraction of accreted material as a function of distance from the Sun, but plots of individual simulations show that this is frequently not the case for any given run. Thus the Earth may have irregularly sampled different regions of the inner Solar System, an issue that would be important if strong compositional gradients existed among planetary building blocks. An average of only 3% $\pm$ 4% (one standard deviation) of the Earths' mass in EJS simulations originated outside of 2.5 AU, while 10% $\pm$ 7% of the Earth analogues' mass in CJS simulations did (Fig. 6). This likely causes the higher water contents of the Earth analogues seen in CJS simulations as compared to EJS simulations (Section 3.1.3). The average timing of the delivery of hydrated material (originating from outside of 2.5 AU) is 13.1 $\pm$ 11.2 Ma for EJS simulations and 15.8 $\pm$ 8.8 Ma for CJS simulations. An average of 29% and 49% of hydrated material accreted by the Earth originated as embryos in EJS and CJS simulations, respectively, with the remainder as planetesimals.

We can also quantify the provenance of the late veneer accreted by the Earth analogue in our simulations. The distribution of source regions of the late veneer varies from simulation to

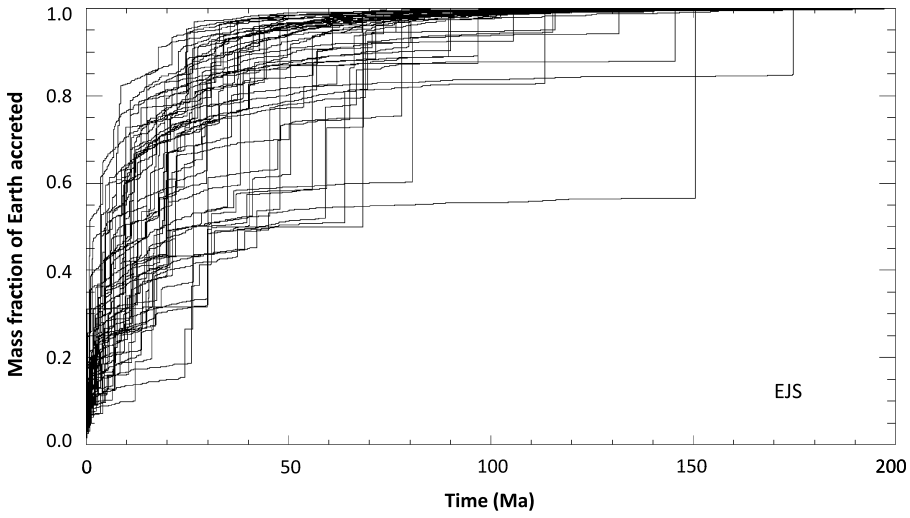

Fig. 4. Mass evolution of the Earth analogues produced in our fifty EJS simulations.

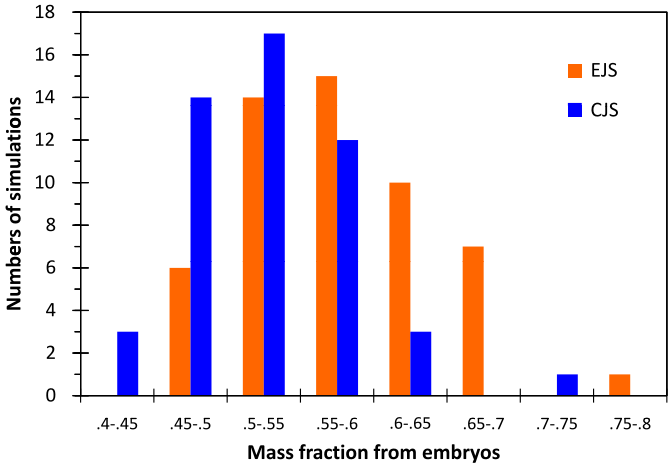

Fig. 5. Mass fraction of Earth analogues from planetary embryos in EJS (orange) and CJS (blue) simulations. (For interpretation of the references to color in this figure legend, the reader is referred to the web version of this article.)

simulation, but differences in the dynamic environments are evidenced by differences between the average distributions for EJS versus CJS simulations (Supplemental Fig. 2). On average, nearly half of the late veneer mass in EJS simulations originated in the range 1–1.5 AU from the Sun, with much less material originating inside 1 AU and a monotonic decrease with increasing distance beyond 1.5 AU. In contrast, CJS simulations show a mostly flat distribution of source regions on average, with approximately half of the late veneer mass originating inside of 2 AU and half originating outside of 2 AU. EJS simulations also show a lower degree of variation in late veneer source distributions between runs than CJS simulations do. In general, this suggests that circular orbits of the giant planets are likely to lead to a more volatile-rich late veneer than the eccentric orbits.

By running a large number of simulations, we are able to illustrate the importance of quantifying the probabilities of rare events. Due to the highly stochastic nature of planetary accretion, it is unknown if various aspects of the Solar System represent the most likely outcomes of its initial conditions. Our results suggest that there is no simple definition of a most likely outcome, but rather that the range of possible outcomes is huge. Therefore, when studying terrestrial planetary accretion, perhaps the goal should not be to find a dynamical environment that consistently reproduces all Solar System observables simultaneously, but

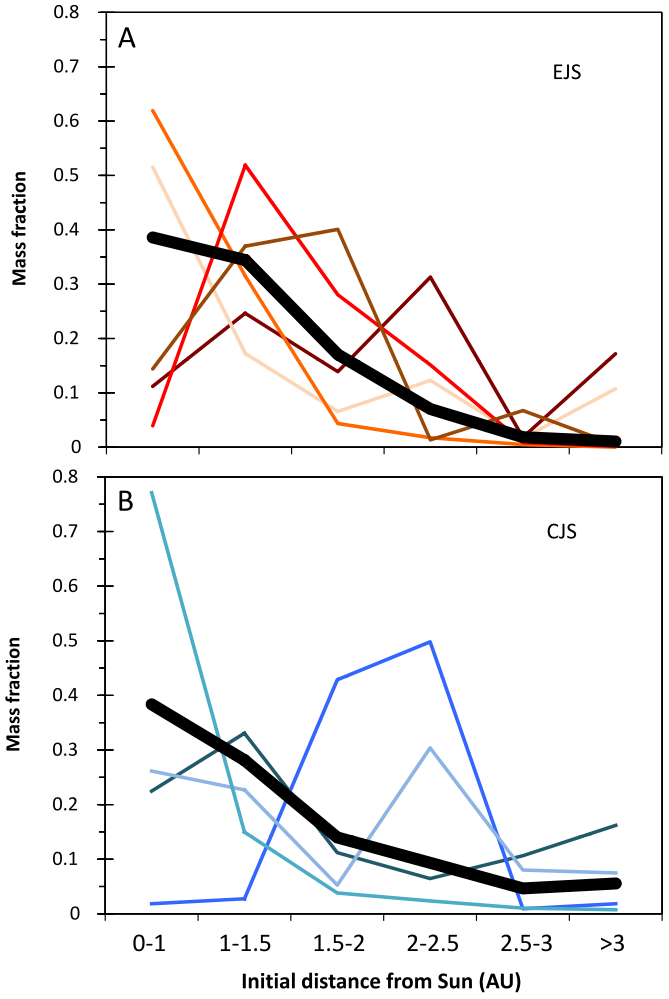

Fig. 6. Distribution of source regions of material accreted by Earth analogues in A: EJS simulations and B: CJS simulations. Thick black line: average over fifty runs. Thin colored lines: examples of a few individual simulations to illustrate the range of outcomes.

rather environments that can match various observables with some probabilities and that do not exhibit strong correlations that would prevent the combination of parameters that describe the Solar System today. If a given environment can be defined that reproduces

all Solar System properties (e.g., Table 1), this would certainly be a strong candidate for representing the conditions present in the early Solar System. However, given the stochastic nature of accretion, when evaluating a given dynamical environment for our Solar System, we must recognize that reproducing all features of the Solar System is unlikely particularly if some outcomes may be low probability events. Only by examining a large number of cases will it be determined what the full range of outcomes for a given dynamical environment is, and consequently whether such an environment is a candidate for the early Solar System. It should also be noted that even if one simulation were to reproduce all Solar System observables simultaneously, this does not necessarily imply that the initial conditions used in that simulation exactly match those of our Solar System.

4. Conclusions

Fifty high-resolution N-body simulations have been run for each of two possible Solar System orbital configurations, with Jupiter and Saturn on either circular or eccentric orbits, to quantify the range of outcomes that are possible in each. These simulations allow quantification of the probabilities of matching dynamic observables of the Solar System, including the likelihood of low probability events, and the correlations that exist between various outcomes. The most strongly correlated Solar System observables are the mass of the late veneer and the formation timescale of the Earth, which can be explained on physical grounds. Most other variables are weakly correlated or uncorrelated, indicating that our simulations may be sampling the full probability distribution functions for the outcomes of individual Solar System observables even if not all of the observed properties are reproduced in any given run. Simulations run with an EJS configuration are approximately ten times more likely to match all Solar System observables tested than those with CJS configurations, though probabilities are still very low for each. However, as stated above, because of the weak to non-existent correlations that were found between the different outcomes described here, failure to reproduce one or multiple observables does not mean other features of the Solar System cannot be produced in the same simulation. Thus, as each of the observables considered here can be reproduced in these dynamic environments, each of the dynamic environments must be considered as plausible for the early Solar System. As such, each of the accretion histories predicted for the Earth analogue should be considered as a possible description of the Earth's true growth history.

N-body simulations provide a wealth of information about planetary growth, such as mass evolution pathways of planets and original sizes and locations of accreted bodies, which has the potential to greatly inform our understanding of the chemistry of the terrestrial planets, and this utility is not limited to simulations whose outcomes closely match the properties of the Solar System. Instead, all of the N-body simulations performed here for the early evolution of our Solar System should be considered as providing possible accretion pathways for the formation and evolution of the Earth that may be realized for a given dynamic scenario. As we advance N-body simulations as tools for studying the chemistry of planetary formation, we must thus consider the full range of accretional histories each dynamic environment might produce in order to ensure a proper comparison of model predictions to geochemical data.

Acknowledgements

We thank John Chambers for useful discussions. We also thank two anonymous reviewers for their constructive feedback. This material is based upon work supported by a National Science Foundation (NSF) Graduate Research Fellowship and an Illinois Space Grant Consortium Fellowship to R.A.F, who was also supported by NSF grant EAR-1243846 to Andrew J. Campbell. F.J.C. was supported by grant NNX12AD59G from NASA's Exobiology program.

Appendix A. Supplementary material

Supplementary material related to this article can be found online at http://dx.doi.org/10.1016/j.epsl.2014.02.011.

References

Agnor, C.B., Canup, R.M., Levison, H.F., 1999. On the character and consequences of large impacts in the late stage of terrestrial planet formation. Icarus 142, 219–237.

Albarede, F., Ballhaus, C., Blichert-Toft, J., Lee, C.-T., Marty, B., Moynier, F., Yin, Q.-Z., 2013. Asteroidal impacts and the origin of terrestrial and lunar volatiles. Icarus 222, 44–52. http://dx.doi.org/10.1016/j.icarus.2012.10.026.

Alexander, C.M.O'D., Bowden, R., Fogel, M.L., Howard, K.T., Herd, C.D.K., Nittler, L.R., 2012. The provenances of asteroids, and their contributions to the volatile inventories of the terrestrial planets. Science 337, 721–723. http://dx.doi.org/10.1126/science.1223474.

Asphaug, E., 2010. Similar-sized collisions and the diversity of planets. Chem. Erde 70, 199–219. http://dx.doi.org/10.1016/j.chemer.2010.01.004.

Bond, J.C., Lauretta, D.S., O'Brien, D.P., 2010. Making the Earth: Combining dynamics and chemistry in the Solar System. Icarus 205, 321–337. http://dx.doi.org/10.1016/j.icarus.2009.07.037.

Chambers, J.E., 1999. A hybrid symplectic integrator that permits close encounters between massive bodies. Mon. Not. R. Astron. Soc. 304, 793–799.

Chambers, J.E., 2001. Making more terrestrial planets. Icarus 152, 205–224. http://dx.doi.org/10.1006/icar.2001.6639.

Chambers, J.E., 2004. Planetary accretion in the inner Solar System. Earth Planet. Sci. Lett. 223, 241–252. http://dx.doi.org/10.1016/j.epsl.2004.04.031.

Chambers, J.E., 2013. Late-stage planetary accretion including hit-and-run collisions and fragmentation. Icarus 224, 43–56. http://dx.doi.org/10.1016/j.icarus.2013.02.015.

Chambers, J.E., Wetherill, G.W., 1998. Making the terrestrial planets: N-body integrations of planetary embryos in three dimensions. Icarus 136, 304–327.

Cuzzi, J.N., Hogan, R.C., Paque, J.M., Dobrovolskis, A.R., 2001. Size-selective concentration of chondrules and other small particles in protoplanetary nebula turbulence. Astrophys. J. 546, 496–508.

Dauphas, N., Marty, B., 2002. Inference on the nature and the mass of Earth's late veneer from noble metals and gases. J. Geophys. Res. 107, 5129. http://dx.doi.org/10.1029/2001JE001617.

Dauphas, N., Pourmand, A., 2011. Hf–W–Th evidence for rapid growth of Mars and its status as a planetary embryo. Nature 473, 489–492. http://dx.doi.org/10.1038/nature10077.

Elser, S., Meyer, M.R., Moore, B., 2012. On the origin of elemental abundances in the terrestrial planets. Icarus 221, 859–874. http://dx.doi.org/10.1016/j.icarus.2012.09.016.

Fassett, C.I., Minton, D.A., 2013. Impact bombardment of the terrestrial planets and the early history of the Solar System. Nat. Geosci. 6, 520–524. http://dx.doi.org/10.1038/NGEO1841.

Gomes, R., Levison, H.F., Tsiganis, K., Morbidelli, A., 2005. Origin of the cataclysmic Late Heavy Bombardment period of the terrestrial planets. Nature 435, 466–469. http://dx.doi.org/10.1038/nature03676.

Hansen, B.M.S., 2009. Formation of the terrestrial planets from a narrow annulus. Astrophys. J. 703, 1131–1140. http://dx.doi.org/10.1088/0004-637X/703/1/1131.

Johansen, A., Oishi, J.S., Mac Low, M.-M., Klahr, H., Henning, T., Youdin, A., 2007. Rapid planetesimals formation in turbulent circumstellar disks. Nature 448, 1022–1025. http://dx.doi.org/10.1038/nature06086.

Karato, S.-i., 2011. Water distribution across the mantle transition zone and its implications for global material circulation. Earth Planet. Sci. Lett. 301, 413–423. http://dx.doi.org/10.1016/j.epsl.2010.11.038.

Krasinsky, G.A., Pitjeva, E.V., Vasilyev, M.V., Yagudina, E.I., 2002. Hidden mass in the asteroid belt. Icarus 158, 98–105. http://dx.doi.org/10.1006/icar.2002.6837.

Laskar, J., 1997. Large scale chaos and the spacing of the inner planets. Astron. Astrophys. 317, L75–L78.

Leinhardt, Z.M., Richardson, D.C., Lufkin, G., Haseltine, J., 2009. Planetesimals to protoplanets – II. Effect of debris on terrestrial planet formation. Mon. Not. R. Astron. Soc. 396, 718–728. http://dx.doi.org/10.1111/j.1365-2966.2009.14769.x.

Lissauer, J.J., 2007. Planets formed in habitable zones of M dwarf stars probably are deficient in volatiles. Astrophys. J. 660, L149–L152.

Mann, U., Frost, D.J., Rubie, D.C., Becker, H., Audétat, A., 2012. Partitioning of Ru, Rh, Pd, Re, Ir, and Pt between liquid metal and silicate at high pressures and high temperatures—Implications for the origin of highly siderophile element concentrations in the Earth's mantle. Geochim. Cosmochim. Acta 84, 593–613. http://dx.doi.org/10.1016/j.gca.2012.01.026.

Minton, D.A., Malhotra, R., 2009. A recored of planet migration in the main asteroid belt. Nature 457, 1109–1111. http://dx.doi.org/10.1038/nature07778.

Minton, D.A., Malhotra, R., 2011. Secular resonance sweeping of the main asteroid belt during planet migration. Astrophys. J. 732, 53. http://dx.doi.org/10.1088/0004-637X/732/1/53.

Morbidelli, A., Chambers, J., Lunine, J.I., Petit, J.M., Robert, F., Valsecchi, G.B., Cyr, K.E., 2000. Source regions and timescales for the delivery of water to the Earth. Meteorit. Planet. Sci. 35, 1309–1320.

Morbidelli, A., Levison, H.F., Tsiganis, K., Gomes, R., 2005. Chaotic capture of Jupiter's Trojan asteroids in the early Solar System. Nature 435, 462–465. http://dx.doi.org/10.1038/nature03540.

Morbidelli, A., Lunine, J.I., O'Brien, D.P., Raymond, S.N., Walsh, K.J., 2012. Building terrestrial planets. Annu. Rev. Earth Planet. Sci. 2012 (40), 251–275. http://dx.doi.org/10.1146/annurev-earth-042711-105319.

Morgan, J.W., 1986. Ultramafic xenoliths: Clues to Earth's late accretionary history. J. Geophys. Res. 91, 12375–12387.

Morishima, R., Stadel, J., Moore, B., 2010. From planetesimals to terrestrial planets: *N*-body simulations including the effects of nebular gas and giant planets. Icarus 207, 517–535. http://dx.doi.org/10.1016/j.icarus.2009.11.038.

Nimmo, F., Kleine, T., 2007. How rapidly did Mars accrete? Uncertainties in the Hf–W timing of core formation. Icarus 191, 497–504. http://dx.doi.org/10.1016/j.icarus.2007.05.002.

O'Brien, D.P., Morbidelli, A., Levison, H.F., 2006. Terrestrial planet formation with strong dynamical friction. Icarus 184, 39–58. http://dx.doi.org/10.1016/j.icarus.2006.04.005.

Raymond, S.N., Quinn, T., Lunine, J.I., 2004. Making other Earths: Dynamical simulations of terrestrial planet formation and water delivery. Icarus 168, 1–17. http://dx.doi.org/10.1016/j.icarus.2003.11.019.

Raymond, S.N., Quinn, T., Lunine, J.I., 2006. High-resolution simulations of the final assembly of Earth-like planets I. Terrestrial accretion and dynamics. Icarus 183, 265–282. http://dx.doi.org/10.1016/j.icarus.2006.03.011.

Raymond, S.N., O'Brien, D.P., Morbidelli, A., Kaib, N.A., 2009. Building the terrestrial planets: Constrained accretion in the inner Solar System. Icarus 203, 644–662. http://dx.doi.org/10.1016/j.icarus.2009.05.016.

Raymond, S.N., Schlichting, H.E., Hersant, F., Selsis, F., 2013. Dynamical and collisional constraints on a stochastic late veneer on the terrestrial planets. Icarus 226, 671–681. http://dx.doi.org/10.1016/j.icarus.2013.06.019.

Rubie, D.C., Frost, D.J., Mann, U., Asahara, Y., Nimmo, F., Tsuno, K., Kegler, P., Holzheid, A., Palme, H., 2011. Heterogeneous accretion, composition and core-mantle differentiation of the Earth. Earth Planet. Sci. Lett. 301, 31–42. http://dx.doi.org/10.1016/j.epsl.2010.11.030.

Schlichting, H.E., Warren, P.H., Yin, Q.-Z., 2012. The last stages of terrestrial planet formation: Dynamical friction and the late veneer. Astrophys. J. 752, 8. http://dx.doi.org/10.1088/0004-637X/752/1/8.

Touboul, M., Kleine, T., Bourdon, B., Palme, H., Wieler, R., 2007. Late formation and prolonged differentiation of the Moon inferred from W isotopes in lunar metals. Nature 450, 1206–1209. http://dx.doi.org/10.1038/nature06428.

Tsiganis, K., Gomes, R., Morbidelli, A., Levison, H.F., 2005. Origin of the orbital architecture of the giant planets of the Solar System. Nature 435, 459–461. http://dx.doi.org/10.1038/nature03539.

Walker, R.J., 2009. Highly siderophile elements in the Earth, Moon and Mars: Update and implications for planetary accretion and differentiation. Chem. Erde 69, 101–125. http://dx.doi.org/10.1016/j.chemer.2008.10.001.

Walsh, K.J., Morbidelli, A., Raymond, S.N., O'Brien, D.P., Mandell, A.M., 2011. A low mass for Mars from Jupiter's early gas-driven migration. Nature 475, 206–209. http://dx.doi.org/10.1038/nature10201.

Weidenschilling, S.J., 1977. The distribution of mass in the planetary system and solar nebula. Astrophys. Space Sci. 51, 153–158.

Weidenschilling, S.J., 2003. Radial drift of particles in the solar nebula: Implications for planetesimals formation. Icarus 165, 438–443. http://dx.doi.org/10.1016/S0019-1035(03)00169-6.

Wetherill, G.W., 1980. Formation of the terrestrial planets. Annu. Rev. Astron. Astrophys. 18, 77–113. http://dx.doi.org/10.1146/annurev.aa.18.090180.000453.

Youdin, A.N., Shu, F.H., 2002. Planetesimal formation by gravitational instability. Astrophys. J. 580, 494–505.